KSCE Journal of Civil Engineering (2022) 26(2):606-618
DOI 10.1007/s12205-021-0527-6

pISSN 1226-7988, eISSN 1976-3808
www.springer.com/12205

Geotechnical Engineering

Evolution of Tensile Properties of Compacted Red Clay under Wet and Dry Cycles

Ling Zeng[a], **Hui-Cong Yu**[a], **Qian-Feng Gao**[b], **Jie Liu**[c], **and Zi-Han Liu**[b]

[a]*School of Civil Engineering, Changsha University of Science & Technology, Changsha 410114, China*
[b]*School of Traffic & Transportation Engineering, Changsha University of Science & Technology, Changsha 410114, China*
[c]*School of Hydraulic Engineering, Changsha University of Science & Technology, Changsha 410114, China*

ARTICLE HISTORY

Received 27 March 2021
Revised 13 July 2021
Accepted 26 August 2021
Published Online 28 October 2021

KEYWORDS

Red clay
Tensile strength
Wet-dry cycle
Desiccation crack
Dry density

ABSTRACT

Tensile strength is an important soil parameter that affects the stability of structures built on clayey soils. This paper presents an experimental study of the change of tensile properties of red clay during wet-dry cycles. Cyclic wet-dry tests were performed on compacted red clay specimens with different initial water contents and dry densities. Direct tensile tests and Brazilian split tests were then conducted on these specimens to determine the soil strengths. The effects of initial water content, initial dry density, number of wet-dry cycles, and crack rate on the tensile properties of red clay were investigated. The results demonstrate that the tensile strength of red clay is generally 1.566 times the splitting strength. Both the tensile strength and splitting strength are negatively correlated with the initial water content but are positively correlated with the initial dry density. Because of the presence of desiccation cracks, the tensile strength goes on reducing under wet-dry cycles. The tensile strength can be expressed by a power function of the initial water content, initial dry density, and crack rate. The proposed equation is useful to evaluate the tensile strength of cracked soils subjected to wet-dry cycles.

1. Introduction

Red clay is a high plasticity lateritic soil that is widely distributed in the tropical and subtropical regions such as the south of China (Hunan, Yunnan, Guizhou, and Guangxi). It is often of brown-red, brown-yellow and other similar colors. This type of lateritic soil is formed from carbonate rocks after long complex physical and chemical weathering. In the natural environment, red clay shows strong shrinking and cracking characteristics because it contains numerous hydrophilic clay minerals, resulting in great changes in its physical and mechanical properties (Thyagaraj and Das, 2017; Lyu et al., 2020; Tang et al., 2020). Particularly, the tensile strength of red clay is obviously weakened by cyclic wet and dry environments due to the occurrence of desiccation cracks (Tang et al., 2016; Pasculli et al., 2017). The reduction of tensile strength will cause geotechnical and environmental problems such as the shallow failure of soil slopes, collapse of foundation pits and leakage of landfills (Murray and Tarantino, 2018; Gao et al., 2019).

To date, many researchers have made efforts to understand the cracking behavior of clayey soils on drying paths via laboratory tests, numerical simulations and field observations (Chong, 2010; Yuan et al., 2014; Wan et al., 2018). It was found that the development of desiccation cracks in clayey soils can be divided into three stages, i.e., the initial stage, the primary stage, and the steady-state stage (Li and Zhang, 2011). The crack initiation and propagation are related to the soil properties (e.g., soil strength, specimen geometry, liquid limit and mineral composition of the soil) and external conditions (e.g., boundary constraint, wet-dry cycles, and temperature) (Tang et al., 2011b; Tollenaar et al., 2017b). Generally, the development of desiccation cracks can be effectively restrained by increasing soil strength and specimen thickness or reducing boundary constraint, liquid limit and clay content (Zeng et al., 2019; Lakshmikantha et al., 2012). An increase in the number of wet-dry cycles will cause more desiccation cracks in the soil. For example, Li and Zhang (2011) reported that both the surface crack density and the crack rate increase first and then tend to be stable with an increasing number of wet-dry

CORRESPONDENCE Qian-Feng Gao ✉ qianfeng.gao@csust.edu.cn 🏢 School of Traffic & Transportation Engineering, Changsha University of Science & Technology, Changsha 410114, China

cycles. Tang et al. (2011a) also found that the crack parameters such as the crack intensity factor, mean crack length, mean crack width, and the number of crack segments per unit area were significantly affected by the applied wet-dry cycles. Some theoretical and empirical models were developed to predict the development process of the cracks (Peron et al., 2009, 2013). Costa et al. (2018) proposed theoretical equations to estimate the crack spacing of a thin, long soil layer based on stress relief and energy balance. Using a combined energy and stress approach, Pouya et al. (2019) developed an analytical model of soil desiccation cracking, which allows predicting the crack depth according to crack spacing. Shrestha et al. (2019) modeled the depth of desiccation cracks measured in the field using a semi-empirical procedure based on the isotropic elasticity principle. Since soil is a highly complex material, it is difficult to precisely characterize the cracking process with a simple model of a few parameters (Tang et al., 2011a).

Matric suction occurs in the soil during drying (Gao et al., 2021). Many previous studies showed that desiccation cracks initiate when the tensile stress induced by the matric suction exceeds the tensile strength of the soil (Peron et al., 2009; Tej and Singh, 2013; Wei et al., 2017). Therefore, the matric suction and tensile strength of the soil are the two key factors controlling the development of desiccation cracks. The tensile strength behavior of soil has been a great concern during the past two decades. There are two common categories of test methods to determine the tensile strength of soil: the direct method (e.g., uniaxial tensile test) and the indirect method (e.g., split test and bending test) (Tang et al., 2014). With the aid of these methods, Varsei et al. (2016), Murray and Tarantino (2018), and Kim and Hwang (2003) studied the tensile characteristics of different compacted soils. It was found that the tensile strength of compacted clay is affected by the dry density, pore structure, and soil type. An increase in dry density, clay content, or plasticity index can effectively improve the tensile strength of the soil. In addition, the tensile strength of unsaturated soils is known as a function of matric suction and significantly depends on the water content. For example, Tang et al. (2014) stated that as the water content increases from 4% to 28%, the tensile strength of a lean clay shows an increase followed by a reduction after reaching the maximum. However, the tensile test results of Stirling et al. (2015) showed that the tensile strength of unsaturated compacted glacial till reduces monotonically as the water content increases from 2% to 24%. This discrepancy seems to be caused by the different methods that were used to prepare soil specimens of different water contents in these two studies.

A review of the above research indicates that the desiccation cracks and tensile strength behavior of clayey soils have been separately studied, and the influence of soil strength on desiccation cracking of the soil has been realized. However, less attention has been paid to the weakening effect of produced desiccation cracks on the tensile properties of red clay. For this reason, the evolution of the tensile strength of compacted red clay subjected to wet-dry cycles is investigated from an experimental point of view. Direct tensile tests and Brazilian split tests are conducted to examine the influences of initial water content and initial dry density on the soil strength. Then, the development of desiccation cracks and the evolution of tensile strengths are investigated under wet-dry cycles. Finally, the relationship between the tensile strength and crack rate of red clay is analyzed and quantified.

2. Material Properties

The studied material was a red clay collected from a section of the Changzhi expressway in Changsha City, Hunan Province, China. The soil sample was reddish brown and contained a small amount of sand and plant roots. After impurity removal, air drying, and rolling, the sample was sieved to remove grains larger than 2 mm. The grain size distribution of the soil was then determined based on the sieve analysis and laser granulometric analysis, as shown in Fig. 1. It shows that the red clay contains about 54% fine grains and 46% sand grains. The X-ray diffraction pattern of the soil indicates that the mineral composition of the soil sample includes kaolinite (42.2%), quartz (29.4%), mica (20.2%), and hematite (8.0%) (Fig. 2). The X-ray fluorescence spectrometry revealed that the soil is mainly composed of oxides and salts of silicon, aluminum, iron, potassium and titanium

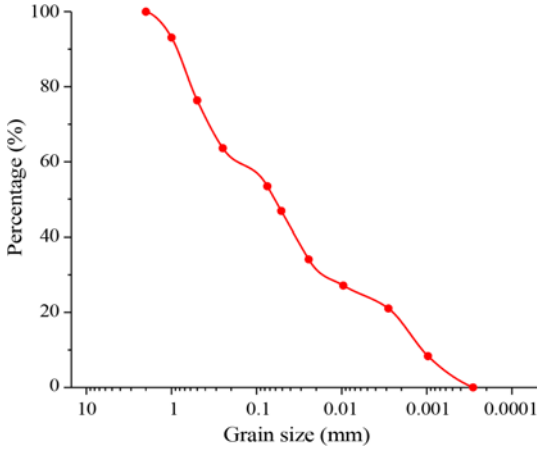

Fig. 1. Grain Size Distribution of Red Clay

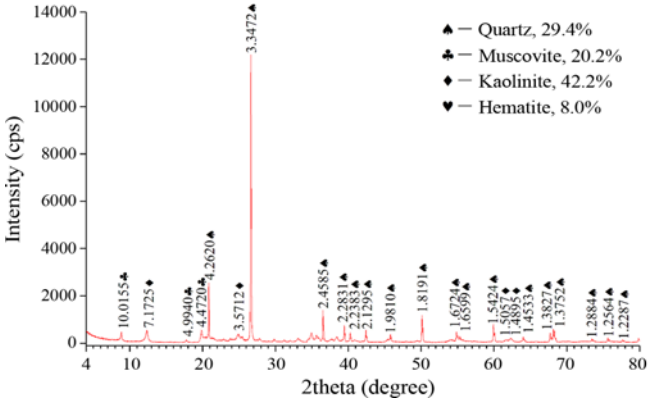

Fig. 2. XRD Diffraction Pattern of Red Clay

Table 1. Chemical Composition of Red Clay

SiO_2	Al_2O_3	Fe_2O_3	K_2O	TiO_2	MgO	P_2O_5	Loss on ignition
57.12	21.27	7.15	2.53	0.88	0.58	0.15	9.98

(Table 1). The basic physical properties of the soil are summarized in Table 2. It shows that the maximum dry density is 1.78 g/cm^3, the optimum water content is 15.5%, the liquid limit is 39.3%, and the plasticity index is 18.7. The soil is classified as low liquid limit clay according to the Chinese specification (JTG 3430-2020, 2020), and it is lean clay (CL) with sand based on the Unified Soil Classification System (USCS).

3. Experimental Methods

3.1 Cyclic Wet-Dry Tests

Cyclic wet-dry tests were conducted to investigate the influences of water content and dry density on the development of desiccation cracks in compacted red clay. For this purpose, two groups of red clay specimens were prepared. The specimens (A1-A6) in the first group have six different initial water contents (2 – 19%) but the same initial dry density (1.78 g/cm^3). The specimens (B1-B4) in the second group have the same initial water content (15.5%) but four different initial dry densities (1.50 – 1.78 g/cm^3). The test scheme is presented in Table 3. The specimen preparation method was as follows: 1) a certain amount of water was sprayed into the dry soil to bring the water content of the soil to the optimum water content; 2) the wet soil was mixed and then cured in a plastic bag for 24 h; 3) the mass of wet soil required for each specimen was calculated according to the desired initial dry density and the specimen volume; 4) the required wet soil was poured into a specimen mold and compressed statically by a press machine with the specimen thickness controlled; 5) when the mold was removed, a red clay specimen of the optimum water content was obtained; 6) different initial water contents were achieved by air drying or wetting the specimens at room temperature (20 ± 1°C), which is similar to the method used by Stirling et al. (2015). The specimen was dumbbell-shaped to facilitate the subsequent direct tensile tests (Tollenaar et al., 2017a; Li et al., 2019). Fig. 3 presents the dimension of the specimen, which is close to that used by Tang et al. (2014).

Many previous studies showed that the electrical conductivity of soil is dependent on the water content and dry density (Oh et al., 2014). Thus, the electrical conductivity of the prepared specimens was tested to evaluate their water contents and dry densities. If the measured electrical conductivity of the specimens prepared at the same initial water content and dry density showed large differences, these specimens were discarded and new specimens were prepared to reduce the error caused by specimen preparations.

Table 3. Cyclic Wet-Dry Test Scheme

Scheme	Initial water content (%)	Initial dry density (g/cm^3)	Number of wet-dry cycles
A1	2.0	1.78	0, 2, 4, 6, 8
A2	5.0	1.78	
A3	10.0	1.78	
A4	15.0	1.78	
A5	17.0	1.78	
A6	19.0	1.78	
B1	15.5	1.50	
B2	15.5	1.60	
B3	15.5	1.70	
B4	15.5	1.78	

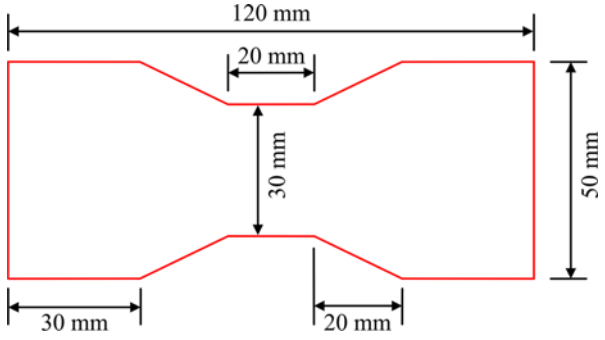

Fig. 3. Dimension of the Dumbbell-Shaped Soil Specimen

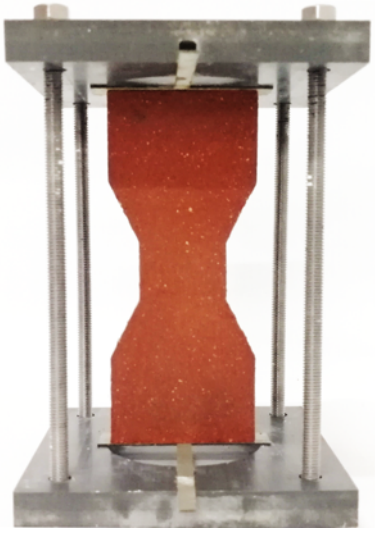

Fig. 4. Specimen Installation in Electric Conductivity Tests

Table 2. Basic Physical Properties of Red Clay

Natural water content (%)	Specific gravity	Maximum dry density (g/cm^3)	Optimum water content (%)	Plastic limit (%)	Liquid limit (%)	Plasticity index
20.8	2.69	1.78	15.5	20.6	39.3	18.7

The two-electrode method was adopted in the electrical conductivity tests. As shown in Fig. 4, metal conductive sheets were fixed on the two ends of dumbbell-shaped specimens, and then the resistance value of the specimen was measured with an ohmmeter. The resistance range of the ohmmeter is 0 – 200 MΩ, and the accuracy is 0.01 MΩ. The electrical conductivity is calculated by the following equation:

$$\eta = \frac{L}{AR}, \tag{1}$$

where η is the electrical conductivity; L is the length of the specimen; R is the measured resistance value; A is the cross-sectional area of the specimen.

During the cyclic wetting-drying process, the water content of red clay specimens ranged between about 0.5% and 25% (Fig. 5), which is similar to those used by Hu et al. (2020). The water film transfer method and lamp heating method were used to make the wet-dry cycles as similar as possible to the natural situation (Meng and Li, 2019; Zeng et al., 2020, 2021a, 2021b). A duration of 24 h was used as the termination criterion for both the wetting process and the drying process. In the wetting process, the red clay specimens were placed on an electronic balance with a precision of 0.01 g, and a predetermined amount of water was evenly dropped on the specimen surfaces by a plastic dropper to make the water content reach 25 ± 0.5%. Before dropping water, a saturated filter paper was placed on the specimen surface to better spread the water on the whole surface of the specimen. The water content was controlled by measuring the mass of the specimen. Then, the specimens were transferred on a stainless steel tray and sealed with a plastic film for curing for 24 h. The uniformity of moisture in the specimen was checked by testing the water contents of the pieces of the parallel specimens using the oven-drying method. In the drying process, the specimens were placed on the tray with a large filter paper on the bottom, and two 250 W heating lamps were used to irradiate the specimens

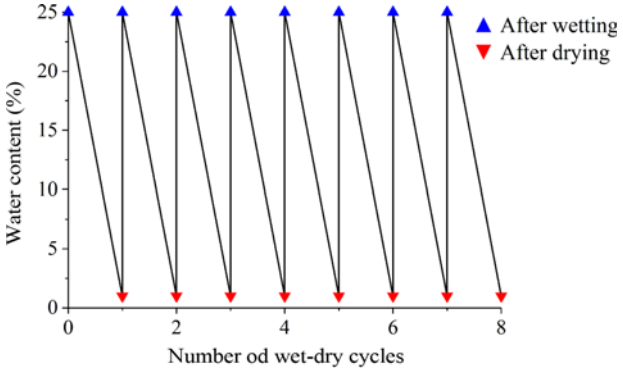

Fig. 5. Diagram of Target Water Contents during Wet-Dry Cycles

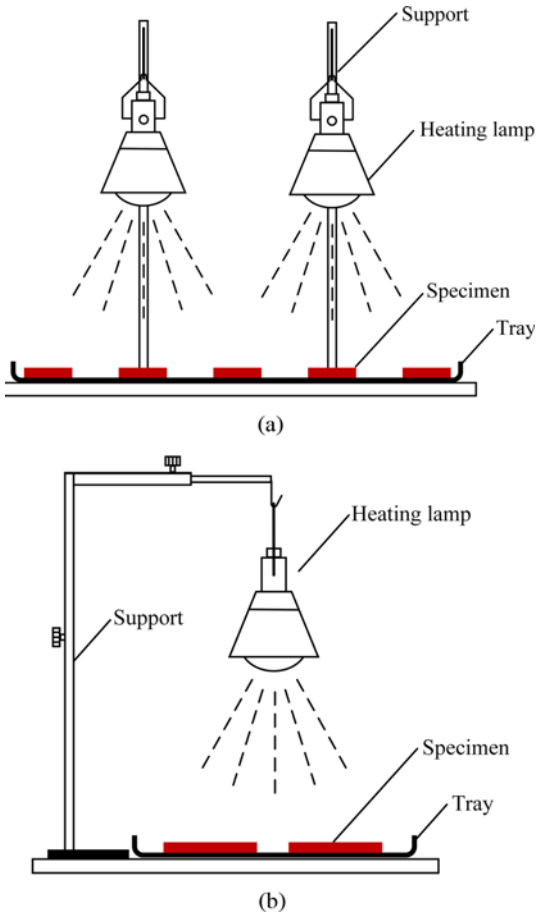

Fig. 6. Drawing of the Specimen Drying Device: (a) Front View, (b) Lateral View

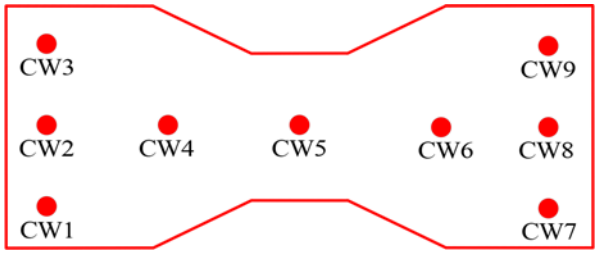

Fig. 7. Temperature Measurement Points on Each Specimen

for 24h (see Fig. 6), resulting in a water content of about (1 ± 0.5)%. The purpose of the filter paper was to create a rough bottom boundary of the specimens.

Since the ground temperature in the studied area (Hunan Province, China) can reach 40°C in summer, the temperature of the specimen surfaces was maintained at 40 ± 1°C in the drying process. The control of the temperature on the specimen surfaces was realized by adjusting the support of the lamps. The heating

Table 4. Average Temperature on the Surfaces of Specimens

Scheme	A1	A2	A3	A4	A5	A6	B1	B2	B3	B4
Average temperature (°C)	39.6	39.9	40.2	39.9	39.7	39.7	40.0	40.4	40.0	39.5

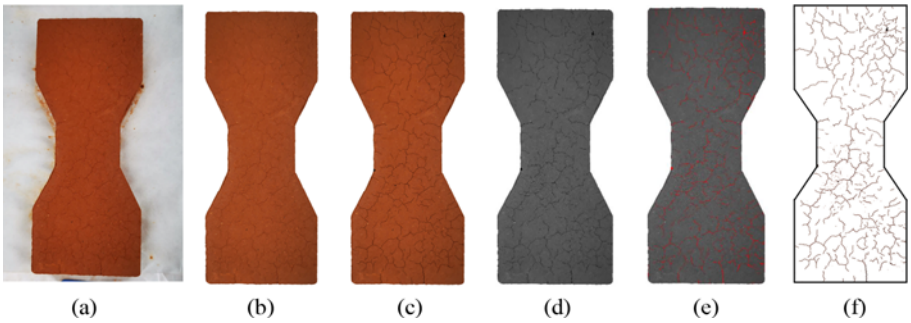

Fig. 8. Image Processing Method: (a) Original Image, (b) Background-Removed Image, (c) Enhanced Image, (d) Grayscale Image, (e) Threshold, (f) Crack Extraction

uniformity was checked before cyclic wet-dry tests. The temperature at nine points (Fig. 7) on each specimen was measured using an electronic temperature gun. The average temperature of each specimen is shown in Table 4. It can be seen that the average temperature of every specimen is 40 ± 1°C, indicating that the heating uniformity of the drying device is satisfactory.

A digital camera installed on a tripod was used to photograph the specimens at a fixed height. Since this section mainly focuses on the influence of wet-dry cycles on crack development, the photograph of the specimen was only taken after each wet-dry cycle. The desiccation cracks were then characterized by analyzing the photographs using the image processing method: 1) the background of the specimen was removed from the original image (Figs. 8(a) and 8(b)); 2) the desiccation cracks on the specimen surface were enhanced by adjusting the brightness and contrast of the image (Fig. 8(c)); 3) the color image was converted into the grayscale image (Fig. 8(d)); 4) the desiccation cracks were extracted from the grayscale image by setting an appropriate threshold (Figs. 8(e) and 8(f)); 5) the crack area and the area of the upper specimen surface were measured. In this study, the first and second steps of image processing was performed using Photoshop software, and the rest steps were conducted with ImageJ software. The crack rate is defined as the ratio of the crack area on the upper surface of a specimen to the total area of the upper surface:

$$F = \frac{S_c}{S}, \tag{2}$$

where F is the crack rate; S_c is the crack area; S is the area of the upper surface of the specimen.

3.2 Direct Tensile Tests

A horizontal tensile test device was designed and manufactured, as shown in Fig. 9. The device consists of a steel frame, a displacement controller, a specimen fixture, a digital force meter, a digital dial indicator, and a computer. The steel frame serves as a support to fix the displacement controller, the specimen fixture, the digital force meter, and the digital dial indicator. The displacement controller is a handwheel and gear system, which enables to control the movement of one-half of the specimen fixture by adjusting the handwheel. The specimen fixture is

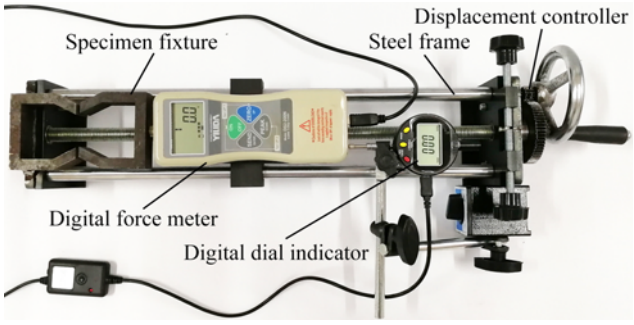

Fig. 9. Direct Tensile Test Device

dumbbell-shaped and made of steel. The measurement range of the digital force meter is 200 N, and the accuracy is 0.1 N. The maximum displacement of the digital dial indicator is 12.7 mm, and the accuracy is 0.01 mm.

With this device, direct tensile tests were performed on dumbbell-shaped specimens when the number of wet-dry cycles reached 0, 2, 4, 6, and 8 (Table 3). The specimen was installed in the fixture, and then the digital force meter and digital dial indicator were reset by the computer. Afterward, the specimen was tested at a displacement rate of 0.5 mm/min (Tang et al., 2014; Tollenaar et al., 2017b). During the test, both the force and displacement were recorded in real-time and saved in the computer. The tensile strength of the red clay specimen is then calculated by the following equation:

$$\sigma_t = \frac{T_m}{A}, \tag{3}$$

where σ_t is the tensile strength; T_m is the maximum tensile force; A is the area of the middle cross-section of the specimen.

After direct tensile tests, the water content of the specimen was measured by the oven-drying method. At the same time, two specimens were tested and the average results were taken for each test scheme to ensure the accuracy of the test results.

3.3 Brazilian Split Tests

The Brazilian split test is a common method to determine the tensile strength of rocks. This method was also used in this study to verify the test results of direct tensile tests. The specimens

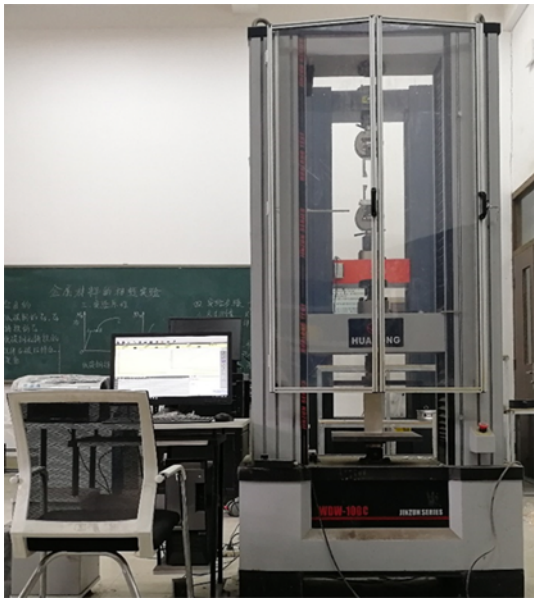

Fig. 10. Universal Testing Machine

were cylindrical and had equal sizes (50 mm) of diameter and height. They were prepared in the specimen mold using the static compression method. The test schemes were the same as those presented in Table 3 but no wet-dry cycles were considered. The Brazilian split tests were conducted using a computer-controlled electronic universal testing machine (Fig. 10). A loading rate of 0.3 MPa/s was applied (JTG E41-2005, 2005), and the ultimate pressure was recorded when the specimen was broken. Thus, the maximum tensile stress in the center of the specimen is calculated by (Komurlu et al., 2015; Xiao et al., 2019):

$$\sigma_{sp} = \frac{2P}{\pi dt}, \tag{4}$$

where σ_{sp} is the maximum tensile stress (or the splitting strength) in the center of the specimen; P is the ultimate pressure when the specimen fails; d and t are the diameter and thickness of the specimen, respectively.

4. Results and Discussion

4.1 Evolution of Desiccation Cracks under Wet-Dry Cycles

Figure 11 presents the photos of a representative red clay specimen after different wet-dry cycles. It is noted that desiccation cracks occur and propagate on the upper surface of the specimen due to wet-dry cycles. The relationship between the crack rate and the number of wet-dry cycles is plotted in Fig. 12. It shows that for the specimens having the same initial water content and dry density, the crack rate monotonically goes up as the number of wet-dry cycles increases. During the drying process, because the heating lamp is located above the specimen, the drying rate on the upper surface of the specimen is faster than that in the lower part. This makes the specimen "dry on top and wet on the bottom", causing a moisture gradient in the specimen. Thus, the matric suction of the upper part of the specimen is greater than that of the lower part, which increases the tensile stress in the upper soil (Lakshmikantha et al., 2012). As a result, desiccation cracks firstly initiate on the upper surface of the specimen. As the number of wet-dry cycles increases, the cracks repeatedly experience a "healing-opening" process, and the existed cracks inside and on the surface of the specimen continue to expand and produce new cracks (Tang et al., 2011a), resulting in a gradual increase in the crack rate. However, the development of desiccation cracks in these specimens is not so significant as that in pure clay slurry (Tang et al., 2011b; Wei et al., 2016). One reason is that the red clay contained many sand grains (Fig. 1), which can reduce the gradients of water content and matric suction in the soil profile during the drying process.

At a given number of wet-dry cycles, the crack rate of the specimen is negatively correlated with the initial water content, and the specimen with an initial water content of 2% has the

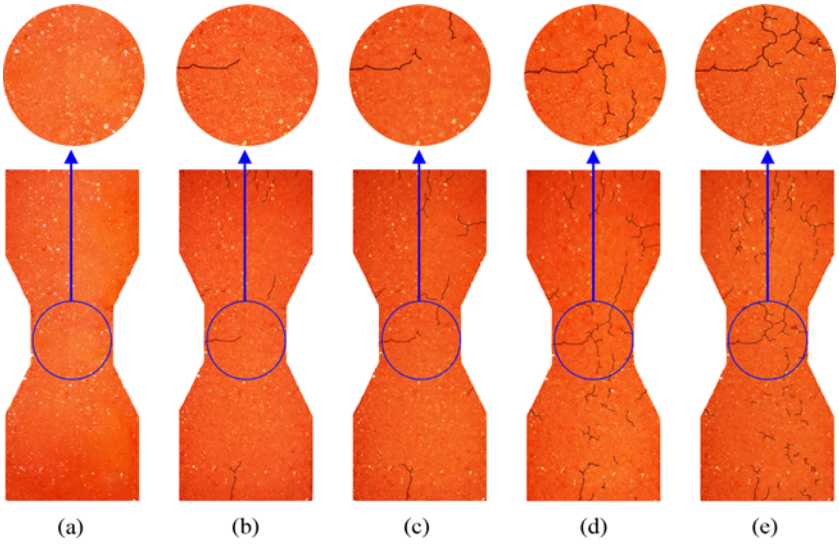

Fig. 11. Desiccation Cracks on the Specimen Surface after Different Wet-Dry Cycles: (a) 0 Cycle, (b) 2 Cycles, (c) 4 Cycles, (d) 6 Cycles, (e) 8 Cycles

largest crack rate. The development of cracks is closely related to the initial defects inside the clay specimen (Costa et al., 2013). Generally, the specimen compacted at a smaller initial water content possesses more initial defects. As a result, the soil structure is more likely to be destroyed and produces more tensile cracks under the action of wet-dry cycles.

Figure 12(a) shows that the slope of the crack rate reduces gradually after six wet-dry cycles when the initial water content is larger than the optimum water content (15.5%). This indicates that the desiccation cracks are less affected by the wet-dry cycles when the specimen has a higher initial water content. The research of Tang et al. (2011a) showed that the influence of wet-dry cycles on soil cracking behavior is related to the soil properties and initial state. When the initial water content is less than the optimum water content, the water in the soil is mainly strongly bound water. In this case, the double-layer force is strong, which prevents soil particles from moving in the wetting process. As a result, the crack healing is poor, and the development of cracks is great in a wet-dry cycle. As the number of wet-dry cycles increases, the existing cracks expand rapidly and more new cracks are created. By contrast, when the initial water content is greater than the optimum water content, the pores in the soil are filled with free water, and the free water acts as lubrication between soil particles. Thus, the cracks show a good healing effect, and the development of cracks is poor in a wet-dry cycle. As the increase in the number of wet-dry cycles, the crack rate grows slowly. And because of the high initial water content, there are fewer defects in the specimen and the specimen has a stronger ability to restrain the development of cracks. In this situation, the increase in crack rate tends to slow down after several cycles.

At a given initial water content, a smaller initial dry density often leads to a greater crack rate of the specimen under wet-dry cycles (Fig. 12(b)). The crack rate reaches the smallest when the specimen is prepared at the maximum dry density. This is because when the initial dry density is small, the soil particles are loosely arranged. Also, the soil porosity is high, and the water is easy to migrate in the soil. Hence, the cracks develop faster, and more new cracks occur during cyclic wetting-drying. When the initial dry density is large, the soil particles are in close contact with each other, so the porosity of the soil is small (Gao et al.,

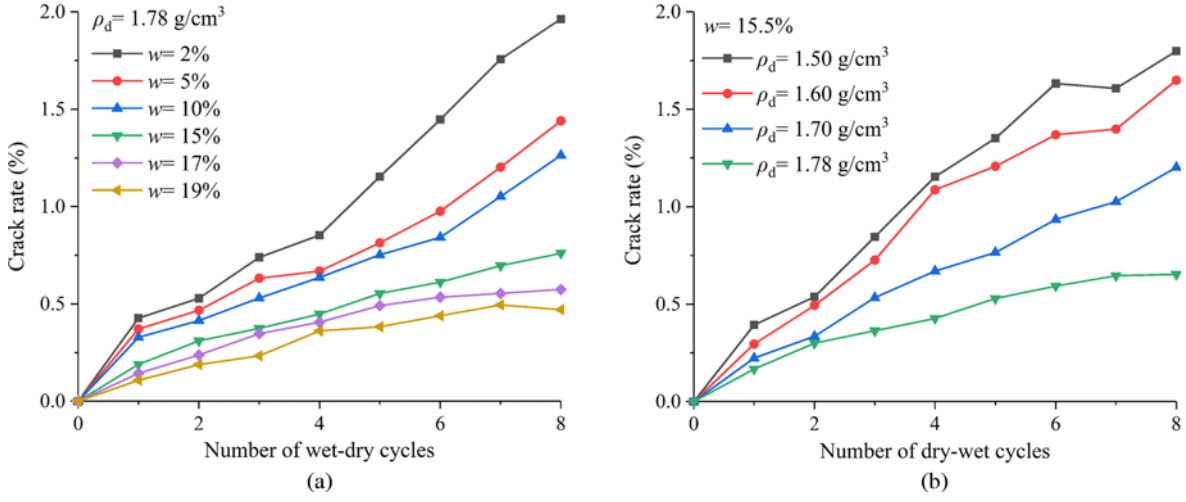

Fig. 12. Relationship between the Number of Wet-Dry Cycles and the Crack Rate: (a) At ρ_d = 1.78 g/cm^3, (b) At w = 15.5%

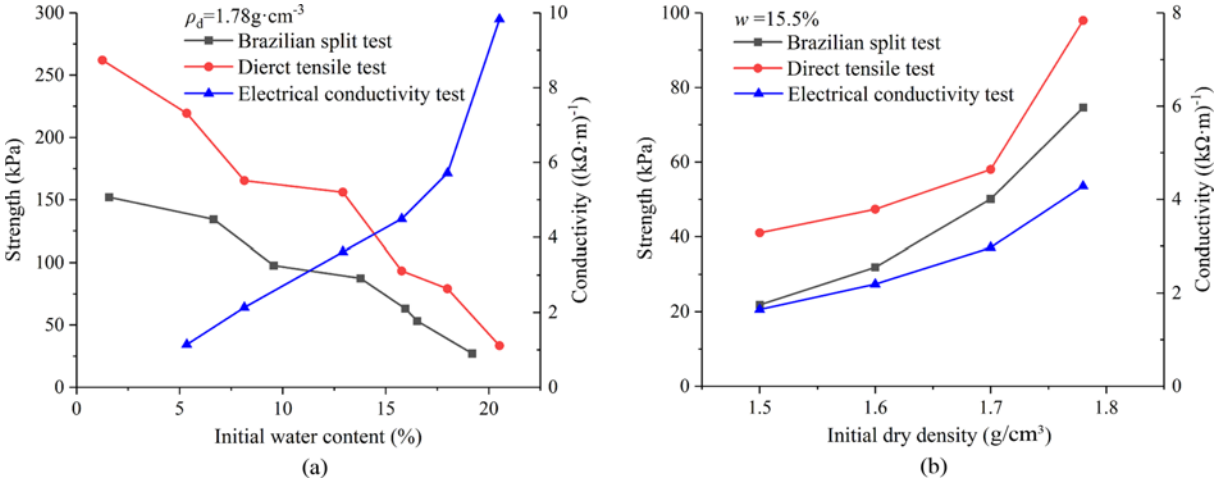

Fig. 13. Tensile Strength and Electrical Conductivity of Intact Specimens Affected by: (a) Initial Water Content, (b) Initial Dry Density

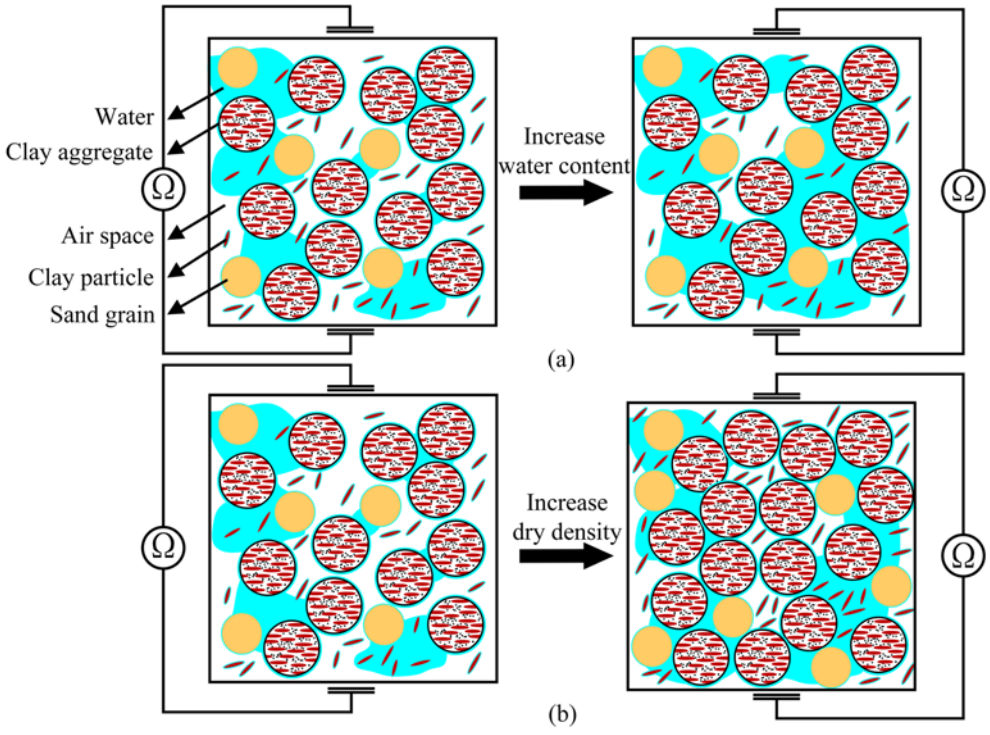

Fig. 14. Mechanism Underlying the Electrical Conductivity Change: (a) Influence of Water Content, (b) Influence of Dry Density

2020). The bonding force between soil particles has a greater inhibitory effect on the development of cracks during the wet-dry cycles. Consequently, the crack rate of the specimen is small. Thus, in addition to the presence of sand grains, another reason why the crack rate of red clay is relatively small is that the specimens used in this study were prepared at large dry densities (Table 3).

4.2 Influences of Initial Water Content and Dry Density on Tensile Strength

Figure 13 shows the electrical conductivity, tensile strength, and splitting strength of intact red clay specimens without suffering from wet-dry cycles. In other words, these properties were measured on wet specimens with water contents between 2% and 19% (Table 3). It is observed that the initial water content and dry density have a great influence on the electrical conductivity of the soil, which is in line with the results of Oh et al. (2014). Generally, the electrical conductivity monotonically increases with the increase in initial water content and dry density. And the electrical conductivity of the specimen is more sensitive to the initial water content than the initial dry density. However, it seems that the electrical conductivity of the red clay specimen is not necessarily related to the tensile strength. Previous studies indicated that there are three types of current flow pathways that contribute to the electrical conductivity of a soil: 1) a liquid phase pathway, 2) a solid-liquid phase pathway, and 3) a solid pathway (Corwin and Lesch, 2005). Among these pathways, the liquid phase containing impurity ions is the main pathway of current flow in the soil (Fig. 14). As an increase in water content or dry density, the three-phase structure of the soil changes, leading to a significant increase in the number of liquid phase pathways or solid pathways. Consequently, the electrical conductivity of the soil increases.

Figure 13 also shows that both the tensile strength and splitting strength of red clay are negatively correlated with the initial water content, which is consistent with the results of Stirling et al. (2015). An increase in water content leads to reductions in capillary force between soil particles and the matric suction of the soil. Hence, the integrity of the soil is weakened, and the tensile strength and splitting strength are reduced. In addition, the tensile strength and splitting strength are positively correlated with the initial dry density. Similar results were obtained by many researchers such as Tollenaar et al. (2017a) and Tang et al. (2014). An increase in dry density leads to a decrease in the volume of pores in the soil and thus causing the soil particles to be tightly contacted. As a result, the electrostatic forces and intermolecular forces between soil particles increase, which is characterized by increases in tensile strength and splitting strength at the macroscopic level. However, the tensile strength of red clay is relatively less than that of pure clay such as kaolinite due to the presence of sand grains (Lu et al., 2007). It is observed from Fig. 15 that the tensile strength can be expressed as a function of the initial water content and initial dry density:

$$\sigma_{t0} = \sigma_0 \frac{\rho_d^n}{w^m}, \tag{5}$$

where σ_{t0} is the tensile strength of intact soil; ρ_d and w are the initial dry density and initial water content of the specimen, respectively; σ_0, n, and m are fitting constants (σ_0 = 3.669, n = 7.691, and m = 0.386 in this study).

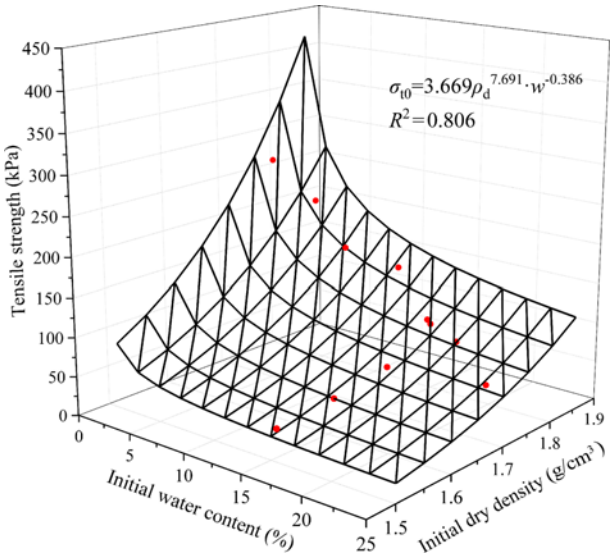

Fig. 15. Relationship between the Tensile Strengths and Initial Parameters of Intact Specimens

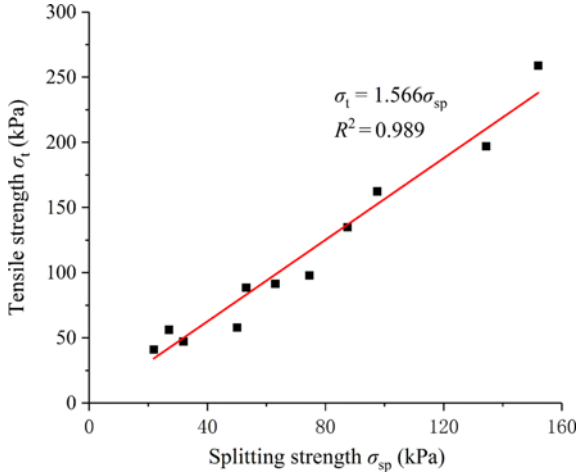

Fig. 16. Relationship between the Tensile Strengths and Splitting Strengths of Intact Specimens

It is found from Fig. 13 that the tensile strength is generally greater than the splitting strength for the specimens prepared at the same initial water content and dry density. And the difference between the two strengths appears to decrease as the initial water content and dry density increase. The curve in Fig. 16 shows that the tensile strength is nearly 1.566 times the splitting strength of the same specimen. The Brazilian split test is an indirect measurement method of the tensile properties of the soil. The specimen not only bears tensile stress but also shear stress during the test, which leads to a faster failure of the specimen and a smaller strength compared to the direct tensile test.

4.3 Influences of Wet-Dry Cycles and Crack Rate on Tensile Strength

After cyclic wet-dry tests, all red clay specimens were dried to a water content of 1 ± 0.5% and showed many desiccation cracks on the surfaces. Direct tensile tests were then conducted on these dried specimens to measure their tensile strengths. Fig. 17 presents the evolution of tensile strength with the increase in wet-dry cycle number. It shows that the tensile strength of the specimen generally reduces as the number of wet-dry cycles increases. The attenuation of tensile strength of the specimen is often the largest in the first two wet-dry cycles. After six wet-dry cycles, the tensile strength tends to be stable as the change is less than 20 kPa. Similar results were obtained by Feng et al. (2020), who investigated the evolution of tensile strength of a collapsed soil subjected to dry-wet cycles by uniaxial tensile tests. Feng et al. (2020) also established a prediction model of the tensile strength attenuation of the soil as an exponential function of the number of dry-wet cycles. Since the way of applying dry-wet cycles may vary in different tests, the number of dry-wet cycles is actually a qualitative indicator. Hence, the model proposed by Feng et al. (2020) cannot be directly used to predict the tensile strength of the soil in this study. Moreover, the tensile strength of

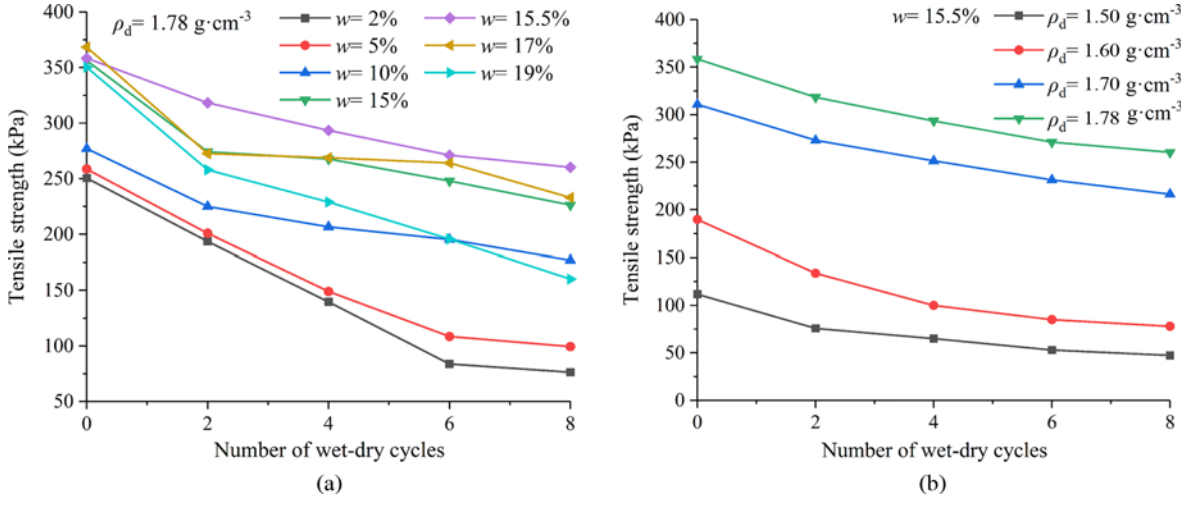

Fig. 17. Relationship between the Tensile Strengths of Cracked Specimens and the Wet-Dry Cycle Number: (a) At ρ_d = 1.78 g/cm³, (b) At w = 15.5%

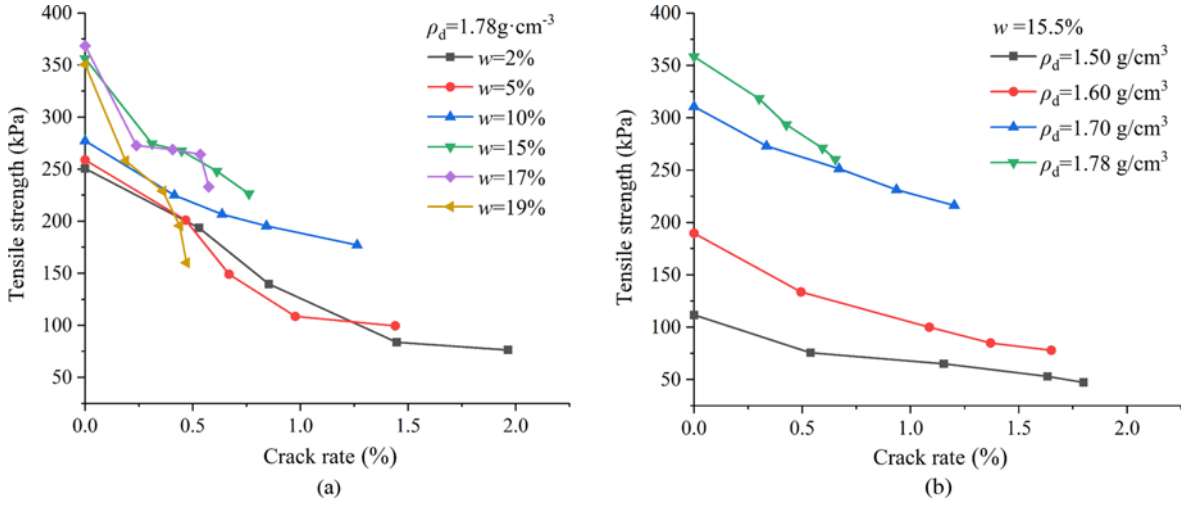

Fig. 18. Relationship between the Crack Rates and Tensile Strengths of Cracked Specimens: (a) At ρ_d = 1.78 g/cm^3, (b) At w = 15.5%

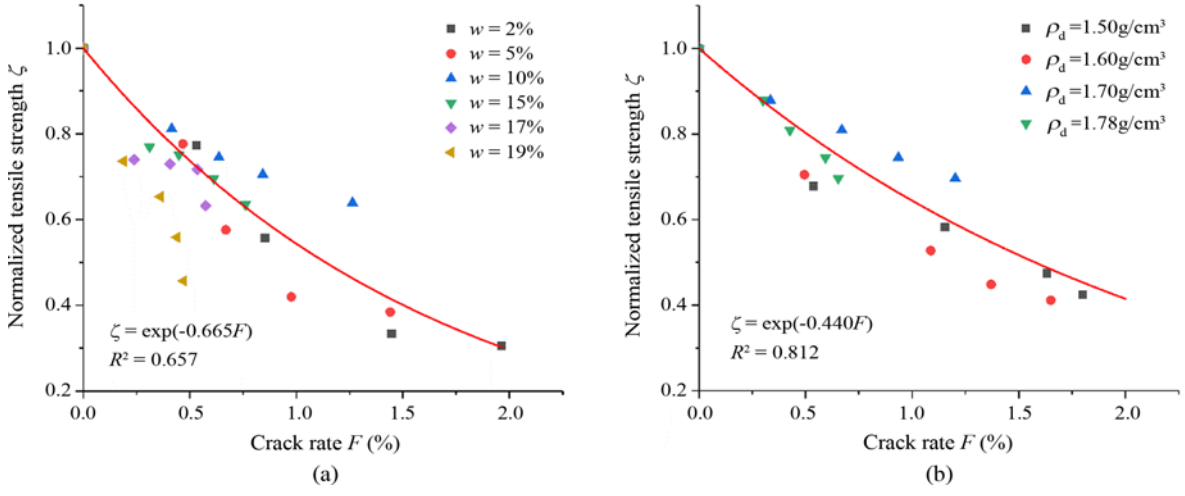

Fig. 19. Relationship between the Normalized Tensile Strengths and Crack Rates of Cracked Specimens: (a) At ρ_d = 1.78 g/cm^3, (b) At w = 15.5%

compacted red clay after several wet-dry cycles exhibits first an increase and then a reduction with increasing initial water content, which is different from that of the intact specimens. The maximum tensile strength appears at the optimum water content of 15.5%. This is reasonable because the specimen has the best internal structure when it is compacted at the optimum water content. In addition, the tensile strength increases with the growth of initial dry density, and the maximum tensile strength occurs at the maximum dry density.

The reason why the number of wet-dry cycles has an influence on the tensile strength of compacted red clay is related to the development of desiccation cracks. Thus, the crack rate is a direct factor determining the tensile strength of the soil. Fig. 18 shows the relationship between the crack rate and the tensile strength under the action of wet-dry cycles. It is observed that the tensile strength of red clay with the same initial condition reduces with the increase in crack rate. The presence of desiccation cracks weakens the integrity of the soil fabric and the bonding between soil particles, resulting in a decrease in tensile strength.

The tensile strengths are normalized by dividing the measured tensile strengths at different crack rates by the measured tensile strength of intact soil with F = 0%:

$$\zeta = \frac{\sigma_t}{\sigma_{t_0}}, \tag{6}$$

where ζ is the normalized tensile strength of cracked soil.

The normalized tensile strengths of the specimens are presented in Fig. 19. It shows that the tensile strength shows first a fast attenuation followed by a slow attenuation and finally an approximation to zero as the crack rate increases. The relationship between the normalized tensile strength and the crack rate can be expressed by an exponential function:

$$\zeta = \exp(aF), \tag{7}$$

where a is a fitting constant.

The form of Eq. (7) is similar to that of the formula proposed by Feng et al. (2020). However, unlike the dry-wet (or wet-dry) cycles, the crack rate is a quantitative indicator, so Eq. (7) is more

practical than the formula of Feng et al. (2020). The coefficient of determination of Eq. (7) is relatively small when the specimens have different initial water contents. This suggests that the attenuation of tensile strength during cyclic wetting-drying is also affected by the initial water content, which is caused by the complex nature of the soil. Combining Eqs. (6) and (7) yields:

$$\sigma_t = \sigma_{t0} \cdot \exp(aF) . \tag{8}$$

Thus, the following equation can be obtained by substituting Eq. (5) into Eq. (8):

$$\sigma_t = \sigma_0 \frac{\rho_d^n}{w^m} \cdot \exp(aF) . \tag{9}$$

Equation (9) describes the tensile strength of cracked soil as a function of the compaction parameters (i.e., ρ_d and w) before wet-dry cycles and the crack rate (F) after wet-dry cycles. This equation provides a simple but useful approach to estimate the tensile strength of red clay. As long as the tensile strength of intact soil is determined, the tensile strength of cracked soil can be conveniently calculated by Eq. (9) based on known crack rate. Notice that the application of Eq. (9) is limited to conditions similar to that used in this study since it is an empirical equation obtained by fitting the test results.

5. Conclusions

In this study, the influences of initial water content and initial dry density on the tensile strength of red clay were examined via direct tensile tests and Brazilian split tests. The development of desiccation cracks and the evolution of tensile strength of the soil were also investigated considering the influence of wet-dry cycles. On this basis, the relationship between the tensile strength and the crack rate of red clay was quantified. The following conclusions can be drawn:

1. Desiccation cracks continuously develop on the surfaces of red clay specimens under wet-dry cycles. However, when the initial water content is larger than the optimum water content, the slope of the crack rate of the specimen tends to reduce after six wet-dry cycles. This is likely because the specimens contain fewer initial defects when they are prepared at a higher water content.
2. The initial water content and initial dry density have significant effects on the tensile properties of compacted red clay. The tensile strength is generally 1.566 times the splitting strength, and both the tensile strength and splitting strength of red clay are negatively correlated with the initial water content but are positively correlated with the initial dry density.
3. Because of the presence of desiccation cracks, the tensile strength of compacted red clay goes on reducing during cyclic wetting-drying. The tensile strength of red clay can be expressed by a power function of the initial water content, initial dry density, and crack rate. This simple equation is useful to evaluate the tensile strength of cracked soils with different initial compaction parameters under wet-dry cycles.

Acknowledgments

The authors gratefully acknowledge the financial support by the National Natural Science Foundation of China (Nos. 51838001, 51878070, 51908069, 51908073, 51978085, and 52008041), and the Changsha Municipal Natural Science Foundation (No. kq2014110).

Nomenclature

A = Cross-sectional area of specimen (mm^2)
d = Diameter of specimen (mm)
F = Crack rate
L = Length of specimen (mm)
P = Ultimate pressure (N)
R = Measured resistance value (kΩ)
S = Specimen area of the upper surface (mm^2)
S_c = Crack area (mm^2)
t = Thickness of specimen (mm)
T_m = Maximum tensile force (N)
w = Initial water content of specimen (%)
ζ = Normalized tensile strength of cracked soil
η = Electrical conductivity ((kΩ·m)$^{-1}$)
ρ_d = Initial dry density of specimen (g/cm^3)
σ_{sp} = Splitting strength (kPa)
σ_t = Tensile strength (kPa)
σ_{t0} = Tensile strength of intact soil (kPa)

ORCID

Ling Zeng http://orcid.org/0000-0001-8167-1049
Hui-Cong Yu http://orcid.org/0000-0003-0174-1700
Qian-Feng Gao http://orcid.org/0000-0003-4844-2345
Jie Liu http://orcid.org/0000-0002-3280-2169
Zi-Han Liu http://orcid.org/0000-0002-9367-6194

References

Chong B (2010) Simulation of crack growth using cohesive crack method. *KSCE Journal of Civil Engineering* 14(5):765-772, DOI: 10.1007/s12205-010-1050-3

Corwin DL, Lesch SM (2005) Apparent soil electrical conductivity measurements in agriculture. *Computers & Electronics in Agriculture* 46(1-3):11-43, DOI: 10.1016/j.compag.2004.10.005

Costa S, Kodikara J, Barbour SL, Fredlund DG (2018) Theoretical analysis of desiccation crack spacing of a thin, long soil layer. *Acta Geotechnica* 13(1):39-49, DOI: 10.1007/s11440-017-0602-9

Costa S, Kodikara J, Shannon B (2013) Salient factors controlling desiccation cracking of clay in laboratory experiments. *Géotechnique* 63(1):18-29, DOI: 10.1680/geot.9.P.105

Feng Y, Zhang X, Ding S, Li B (2020) Analysis of attenuation of tensile strength of collapsing soil under the action of dry and wet cycles. *Journal of Soil and Water Conservation* 34(3):170-176, DOI: 10.13870/j.cnki.stbcxb.2020.03.026 (in Chinese)

Gao QF, Shi ZN, Luo JT, Liu J (2020) Microstructural insight into permeability and water retention property of compacted binary silty

clay. *Journal of Central South University* 27(7):2068-2081, DOI: 10.1007/s11771-020-4431-x

Gao QF, Zeng L, Shi ZN, Zhang R (2021) Evolution of unsaturated shear strength and microstructure of a compacted silty clay on wetting paths. *International Journal of Geomechanics* 21(12), DOI: 10.1061/(ASCE)GM.1943-5622.0002207

Gao QF, Zhao D, Zeng L, Dong H (2019) A pore size distribution-based microscopic model for evaluating the permeability of clay. *KSCE Journal of Civil Engineering* 23(12):5002-5011, DOI: 10.1007/s12205-019-2219-z

Hu CM, Yuan YL, Mei Y, Wang XY, Liu Z (2020) Comprehensive strength deterioration model of compacted loess exposed to drying-wetting cycles. *Bulletin of Engineering Geology and the Environment* 79(1):383-398, DOI: 10.1007/s10064-019-01561-8

JTG 3430-2020 (2020) Test methods of soils for highway engineering. JTG 3430-2020, Ministry of Transport of the People's Republic of China, Beijing, China

JTG E41-2005 (2005) Test methods of rock for highway engineering. JTG E41-2005, Ministry of Transport of the People's Republic of China, Beijing, China

Kim TH, Hwang C (2003) Modeling of tensile strength on moist granular earth material at low water content. *Engineering Geology* 69(3-4):233-244, DOI: 10.1016/S0013-7952(02)00284-3

Komurlu E, Kesimal A, Demir S (2015) An experimental and numerical study on determination of indirect (splitting) tensile strength of rocks under various load apparatus. *Canadian Geotechnical Journal* 53(2), DOI: 10.1139/cgj-2014-0356

Lakshmikantha MR, Prat PC, Ledesma A (2012) Experimental evidence of size effect in soil cracking. *Canadian Geotechnical Journal* 49(3):264-284, DOI: 10.1139/t11-102

Li HD, Tang CS, Cheng Q, Li SJ, Gong XP, Shi B (2019) Tensile strength of clayey soil and the strain analysis based on image processing techniques. *Engineering Geology* 253:137-148, DOI: 10.1016/j.enggeo.2019.03.017

Li JH, Zhang LM (2011) Study of desiccation crack initiation and development at ground surface. *Engineering Geology* 123(4):347-358, DOI: 10.1016/j.enggeo.2011.09.015

Lu N, Wu B, Tan CP (2007) Tensile strength characteristics of unsaturated sands. *Journal of Geotechnical and Geoenvironmental Engineering* 133(2):144-154, DOI: 10.1061/(ASCE)1090-0241(2007)133:2(144)

Lyu H, Gu J, Li W, Liu F (2020) Analysis of compressibility and mechanical behavior of red clay considering structural strength. *Arabian Journal of Geosciences* 13(11):1-11, DOI: 10.1007/s12517-020-05352-4

Meng J, Li XA (2019) Effects of carbonate on the structure and properties of loess and the corresponding mechanism: An experimental study of the Malan loess, Xi'an area, China. *Bulletin of Engineering Geology and the Environment* 78(7):4965-4976, DOI: 10.1007/s10064-018-01457-z

Murray I, Tarantino A (2018) Mechanisms of failure in saturated and unsaturated clayey geomaterials subjected to (total) tensile stress. *Géotechnique* 69(8):1-43, DOI: 10.1680/jgeot.17.p.252

Oh TM, Cho GC, Lee C (2014) Effect of soil mineralogy and pore-water chemistry on the electrical resistivity of daturated doils. *Journal of Geotechnical and Geoenvironmental Engineering* 140(11):06014012, DOI: 10.1061/(ASCE)GT.1943-5606.0001175

Pasculli A, Sciarra N, Esposito L, Esposito AW (2017) Effects of wetting and drying cycles on mechanical properties of pyroclastic soils. *Catena* 156:113-123, DOI: 10.1016/j.catena.2017.04.004

Peron H, Hueckel T, Laloui L, Hu L (2009) Fundamentals of desiccation cracking of fine-grained soils: Experimental characterisation and mechanisms identification. *Canadian Geotechnical Journal* 46(10):1177-1201, DOI: 10.1139/T09-054

Peron H, Laloui L, Hu LB, Hueckel T (2013) Formation of drying crack patterns in soils: A deterministic approach. *Acta Geotechnica* 8(2):215-221, DOI: 10.1007/s11440-012-0184-5

Pouya A, Vo TD, Hemmati S, Tang AM (2019) Modeling soil desiccation cracking by analytical and numerical approaches. *International Journal for Numerical and Analytical Methods in Geomechanics* 43(3):738-763, DOI: 10.1002/nag.2887

Shrestha A, Jotisankasa A, Chaiprakaikeow S, Pramusandi S, Soralump S, Nishimura S (2019) Determining shrinkage cracks based on the small-strain shear modulus-suction relationship. *Geosciences* 9(9):362, DOI: 10.3390/geosciences9090362

Stirling RA, Hughes P, Davie CT, Glendinning S (2015) Tensile behaviour of unsaturated compacted clay soils - A direct assessment method. *Applied Clay Science* 112-113:123-133, DOI: 10.1016/j.clay.2015.04.011

Tang CS, Cheng Q, Leng T, Shi B, Zeng H, Inyang HI (2020) Effects of wetting-drying cycles and desiccation cracks on mechanical behavior of an unsaturated soil. *Catena* 194:104721, DOI: 10.1016/j.catena.2020.104721

Tang CS, Cui YJ, Shi B, Tang AM, Liu C (2011a) Desiccation and cracking behaviour of clay layer from slurry state under wetting–drying cycles. *Geoderma* 166(1):111-118, DOI: 10.1016/j.geoderma.2011.07.018

Tang CS, Pei XJ, Wang DY, Shi B, Li J (2014) Tensile strength of compacted clayey soil. *Journal of Geotechnical and Geoenvironmental Engineering* 141(4):04014122, DOI: 10.1061/(ASCE)GT.1943-5606.0001267

Tang CS, Shi B, Liu C, Suo WB, Gao L (2011b) Experimental characterization of shrinkage and desiccation cracking in thin clay layer. *Applied Clay Science* 52(1-2):69-77, DOI: 10.1016/j.clay.2011.01.032

Tang CS, Wang DY, Shi B, Li J (2016) Effect of wetting–drying cycles on profile mechanical behavior of soils with different initial conditions. *Catena* 139:105-116, DOI: 10.1016/j.catena.2015.12.015

Tej PR, Singh DN (2013) Estimation of tensile strength of soils from penetration resistance. *International Journal of Geomechanics* 13(5):496-501, DOI: 10.1061/(ASCE)GM.1943-5622.0000234

Thyagaraj T, Das AP (2017) Physico-chemical effects on collapse behaviour of compacted red soil. *Géotechnique* 67(7):559-571, DOI: 10.1680/jgeot.15.P.240

Tollenaar RN, Van Paassen LA, Jommi C (2017a) Experimental evaluation of the effects of pull rate on the tensile behavior of a clay. *Applied Clay Science* 144:131-140, DOI: 10.1016/j.clay.2017.04.026

Tollenaar RN, Van Paassen LA, Jommi C (2017b) Observations on the desiccation and cracking of clay layers. *Engineering Geology* 230:23-31, DOI: 10.1016/j.enggeo.2017.08.022

Varsei M, Miller GA, Hassanikhah A (2016) Novel approach to measuring tensile strength of compacted clayey soil during desiccation. *International Journal of Geomechanics* 16(6):D4016011, DOI: 10.1061/(asce)gm.1943-5622.0000705

Wan Y, Xue Q, Liu L, Wang SY (2018) Relationship between the shrinkage crack characteristics and the water content gradient of compacted clay liner in a landfill final cover. *Soils and Foundations* 58(6):1435-1445, DOI: 10.1016/j.sandf.2018.08.011

Wei X, Duc M, Hattab M, Reuschlé T, Taibi S, Fleyreau JM (2017) Effect of decompression and suction on macroscopic and microscopic behavior of a clay rock. *Acta Geotechnica* 12(1):47-65, DOI: 10.1007/s11440-016-0454-8

Wei X, Hattab M, Bompard P, Fleureau JM (2016) Highlighting some mechanisms of crack formation and propagation in clays on drying path. *Géotechnique* 66(4):287-300, DOI: 10.1680/jgeot.14.p.227

Xiao Y, He X, Evans TM, Stuedlein AW, Liu HL (2019) Unconfined compressive and splitting tensile strength of basalt fiber-reinforced biocemented sand. *Journal of Geotechnical and Geoenvironmental Engineering* 145(9):04019048, DOI: 10.1061/(ASCE)GT.1943-5606.0002108

Yuan HN, Peng C, Lin Q, Zhang BY (2014) Simulation of tensile cracking in earth structures with an adaptive RPIM-FEM coupled method. *KSCE Journal of Civil Engineering* 18(11):2007-2018, DOI: 10.1007/s12205-014-1490-2

Zeng L, Liu J, Gao QF, Bian HB (2019) Evolution characteristics of the cracks in the completely disintegrated carbonaceous mudstone subjected to cyclic wetting and drying. *Advances in Civil Engineering* 2019:1-10, DOI: 10.1155/2019/1279695

Zeng L, Luo JT, Liu J, Gao QF, Bian HB (2021a) Disintegration characteristics and mechanisms of carbonaceous mudstone subjected to load and cyclic drying-wetting. *Journal of Materials in Civil Engineering* 33(8), DOI: 10.1061/(ASCE)MT.1943-5533.0003817

Zeng L, Yu HC, Gao QF, Bian HB (2020) Mechanical behavior and microstructural mechanism of improved disintegrated carbonaceous mudstone. *Journal of Central South University* 27(7):1992-2002, DOI: 10.1007/s11771-020-4425-8

Zeng L, Yu HC, Liu J, Gao QF, Bian HB (2021b) Mechanical behaviour of disintegrated carbonaceous mudstone under stress and cyclic drying/wetting. *Construction and Building Materials* 282(6):122656, DOI: 10.1016/j.conbuildmat.2021.122656